Tailoring of RF Coded Optical Pulses for Underwater 3D Imaging

A Comparison of Modulated Pulse Lidar to Traditional Short Pulse Lidar

Justin K. Nash, Robert W. Lee, Linda J. Mullen
Naval Air Systems Command (NAVAIR)
Patuxent River, MD, USA
justin.k.nash@navy.mil

Abstract*— Laser imaging of 3D targets in highly scattering environments has traditionally been done using narrow 1-2ns optical pulses in conjunction with a range-gated detector. While this approach offers range resolution determined by the width of the optical pulse and is very effective in eliminating the effects of backscatter from the turbid environment, it lacks resistance to the effects of forward scatter. The Modulated Pulse Lidar is an alternative approach developed by researchers at NAVAIR that uses longer pulses that are intensity modulated with RF coded waveforms. Radar pulse compression techniques involving the use of RF coded waveforms with large bandwidths provide range resolution that meets or exceeds that of the short pulse approach, while matched-filtering techniques are employed to suppress backscatter. More importantly, the modulated pulse approach provides resistance to forward scatter effects that the short pulse approach does not. This work focuses on the comparison of imagery generated employing both pulse schemes in the same line-scan underwater 3D imaging system over a range of water turbidities. Experimental imagery and temporal data will be presented that shows that the modulated pulse approach does in fact offer an advantage over the short pulse approach due to its resistance to forward scatter effects.

***Keywords*— lidar, modulated pulse, frequency chirp, underwater imaging**

I. Introduction

The approach for traditional laser radar (lidar) imaging uses a short optical pulse (typically 1-2ns) to generate high quality 3D imagery [1,2]. Pixel intensity is determined by the magnitude of the detected signal, and pixel range, which produces depth in the image for 3D perspective, is determined by the time of flight of the detected signal. The range resolution is governed by the width of the optical pulse (i.e. a shorter pulsewidth leads to increased range resolution). Researchers at NAVAIR have been working on an alternative approach to 3D laser imaging that involves the use of modulated optical pulses rather than short pulses [3-6]. This approach uses an optical pulse of longer width (~20ns) that employs intensity modulation to encode the pulse with an RF waveform. Matched-filtering is used to generate a correlation function between the pulse returns and a recorded copy of the outgoing pulse. Here, pixel intensity is determined by the magnitude of the correlation peak while range is determined by the peak's location in time. In this approach, range resolution is determined by the bandwidth of the RF signal encoded on the optical pulse which directly governs the width of the correlation peak in the matched-filter output. By choosing a waveform with sufficiently wide bandwidth through modulation of either the frequency or phase content of the encoded RF signal, the range resolution of the modulated pulse can be made equivalent to that of the short pulse. In non-scattering environments, both the short pulse and modulated pulse approaches at equivalent pulse energies perform equally well.

In turbid media, such as murky water, scattering effects degrade the quality of the 3D imagery. One such effect is backscatter where photons scatter back toward the receiver without ever making it to the intended target. The collection of backscattered light causes loss of image contrast. The short pulse approach mitigates backscatter by gating the receiver such that it does not "open" until the return from the target arrives. Therefore, the receiver ignores the backscattered photons which arrive before the target returns. While gating the receiver is effective at suppressing backscatter, it has two main drawbacks. One disadvantage is that the gating process leaves the receiver blind to any objects of interest before the gate signal is applied. Another drawback is that one must have prior knowledge of the expected range of the target to determine where to place the gate in time.

The modulated pulse approach separates the target and backscatter returns based on their frequency content. The spread in arrival times of the backward-scattered photons washes out the modulation at frequencies exceeding ~100MHz. However, the coherent return from an underwater object retains the encoded modulation signal. By modulating at frequencies >100MHz, the received signal can be high-pass filtered to eliminate the low frequency component of the return due to backscatter. The subsequent matched-filtering process used to determine pixel range and intensity also suppresses high frequency, uncorrelated noise components of the received signal. This backscatter removal technique requires no prior knowledge of expected target range and, in general, no gating electronics on the receiver detector. In the presence of extremely high backscatter, a gate may be necessary to avoid being limited by the dynamic range of the receiver. However,

NISE/Section 219

a gate with lower extinction would suffice since the modulated pulse scheme does not rely solely on the gate to discriminate against backscatter.

The other major effect of scattering in turbid media is multiple small-angle scattering on the path to the object (i.e. forward scatter). Forward scattering causes spreading in the spatial extent of the beam which leads to photons hitting parts of the target other than the intended location. This results in a loss of spatial resolution, as well as a loss of range resolution if the unintended parts of the target are at different ranges. Additionally, multiple forward scattering causes a short optical pulse to be stretched in time, which results in additional loss of range resolution. The short pulse approach has no way to mitigate forward scatter effects except to limit the amount of forward scattered light collected by reducing the receiver field-of-view (FOV). This benefits the modulated pulse scheme equally, but also results in a decrease in signal-to-noise (SNR) as turbidity and/or range to target are increased. Recent research has shown that modulation frequencies >500MHz are capable of discriminating against multiply forward scattered returns [7-10]. The principle behind this is that the higher frequencies become attenuated with multiple scattering events. Thus, when photons that have been multiply scattered are received at the detector they are less correlated with the transmitted signal. This allows the matched-filtering process used in the modulated pulse approach to favor returns that have experienced less forward scatter. Modulated pulse waveforms are tailored to contain these high frequency components to provide a way to mitigate forward scatter without having to limit the receiver field of view. By choosing waveforms that are wideband and include high frequency content, the modulated pulse approach can realize high range resolution, backscatter suppression, and forward scatter resistance simultaneously in a turbid imaging environment.

The focus of this paper is to compare the short pulse and modulated pulse approaches using real underwater 3D imagery produced in a controlled laboratory environment. The goal is to determine the advantages of the modulated pulse approach and if/when those advantages break down in highly scattering environments. Measured experimental imagery will be presented, as well as temporal data to provide insight into differences in the imagery over a range of water turbidities.

II. EXPERIMENTAL SETUP

A Fibertek laser acquired through a Phase II SBIR was used to generate both the short pulses and the modulated pulses employed in these experiments. The laser consisted of a low power seed semiconductor laser that is modulated, fiber-amplified and doubled to 532nm via a non-critically phase-matched LBO crystal. RF encoding of the optical pulses was accomplished by sending binary commands to an FPGA via a software interface. The system can accommodate arbitrarily chosen frequency/phase modulated waveforms with frequency content up to 1GHz. A "macro" pulse of selectable pulsewidth was then amplitude modulated with the RF waveform via a Mach-Zehnder modulator to encode the information. For this work, the RF waveform was a "chirp" with frequency content that was linearly swept from 250-1000MHz encoded on a macro pulse with a width of 20ns. For the short pulse, the smallest acceptable binary command was used to create a singly peaked output pulse with a FWHM pulsewidth of 1.3ns resulting in a bandwidth of 770MHz, which closely matched the 750MHz bandwidth of the modulated chirp pulse.

Data for both short pulse and modulated pulse approaches was collected in synchronous line scan fashion. For a given turbidity the only change to the system was in the temporal profile of the laser pulses. The laser pulses were directed into the water tank and at the 3D target for imaging via a rotating polygon scanner. In traditional synchronous scan manner, the laser and photomultiplier tube (PMT) detector were aligned relative to the polygon such that the center of the FOV of the PMT was co-located with the laser spot at all times throughout the scan. With the six-sided polygon rotating at 1000rpm (6000deg/s) and laser operating at a pulse repetition frequency (PRF) of 509kHz, the angular separation between successive laser shots was 0.012deg. At a nominal target distance of 7.5m, this leads to a shot-to-shot separation of 1.646mm. Collimating and focusing optics were used to achieve a laser spot size of ~3mm on target. The lateral extent of the target was such that 456 pixels were acquired for each row of the image. The FOV of the PMT was fixed at 1.146deg (full width) leading to a 150mm diameter footprint on the target. The PMT, manufactured by Photonis (model #QS19413-1), had five stages and was specially designed for a response from DC-1GHz. The laser and receiver had an effective separation of 29cm.

Each row of a 3D image was formed by a horizontal scan of the polygon across the target. The time-amplitude data for all 456 pixels was digitized at 5GSPS by a LeCroy WaveRunner oscilloscope. A LabView GUI processed and stored the return pulse and a reference pulse for each pixel. The reference pulse was a measurement of the actual outgoing laser pulse taken before entering the water channel. After all the row data was acquired, stored, and processed, a vertical translation stage to which the target was attached moved the target vertically by 10mm for the next row of the image. The vertical extent of the target accommodated 45 rows of pixels at the 10mm spacing.

The target itself consisted of two range features, a cone and a "wedding cake" (three concentric cylinders of varying diameter) mounted to a flat backboard. A photograph and a schematic with dimensions are given in Fig. 1. The entire target was painted matte gray for a uniform reflectivity (i.e. intentionally low contrast).

Turbidity of the water (i.e. the density of scatterers that influences the forward and backscatter properties of the water channel) was varied by introduction of Equate antacid solution into the water tank. The beam attenuation coefficient, c, that characterizes the attenuation of an optical signal due to absorption and scattering in the medium was measured with an in-situ transmissometer at the 532nm laser wavelength. For these experiments no absorption was introduced, hence the magnitude of c was due solely to scattering effects. The attenuation length (denoted cz) is defined as the product of the attenuation coefficient and the physical range, z. In these experiments, $z = 7.5$m.

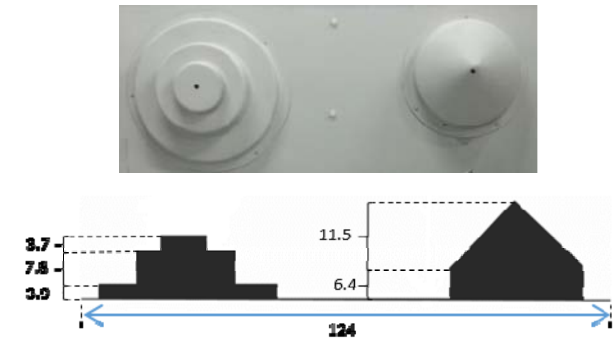

Fig. 1. Photograph of target (top) used in the experiments as viewed by the laser imaging system, and schematic with dimensions in cm (bottom). The feature on the left will be referred to as the “wedding cake”, and the feature on the right as the “cone”.

For each pulse scheme the laser power into the tank was adjusted to maximize the peak amplitude of the target component of the return pulse up to a limit of 300mV (the maximum extent of the PMT’s linear response). Due to the lower peak power of the longer modulated pulses, a greater amount of average laser power was needed to achieve the maximum 300mV peak return signal level relative to the short pulse. Furthermore, since the same nonlinear crystal was used for conversion of both the short and modulated pulses to 532nm, a lower maximum average laser power was achievable with the modulated pulses. Therefore, above a certain turbidity less maximum signal was attainable with the modulated pulses using all of the laser power. At each turbidity, the short pulse signal levels were maximized (up to the 300mV limit) rather than limiting them to that of the modulated pulse signal levels. This gave the short pulse an advantage from an SNR perspective, but one that is inherent in a given laser system due to the difference in pulsewidths. The difference could be eliminated by using a higher power fundamental source for generation of modulated pulses, or by using a periodically-poled nonlinear crystal for doubling of the modulated pulse, but both would increase the complexity of the system. The actual signal levels obtained and the corresponding average powers are given in Fig. 2.

III. DATA AND PROCESSING

A. Modulated Pulse

As described above, time-amplitude temporal data of a reference pulse and a return pulse were acquired, digitized and stored for each pixel in the image. Enough temporal history was captured to encompass the backscatter and target components of the return signals. For the modulated pulse scheme, the return and reference signals were first preprocessed using a digital high-pass filter with a 150MHz cut-off to eliminate any DC component of the target and backscatter portions of the return, as well as any low frequency noise components. A matched filter operation was then performed using the AC-coupled signals (i.e. a cross-correlation between the reference and return). The intensity of the pixel was determined by the amplitude of the peak in the matched-filter output. The range was determined by the

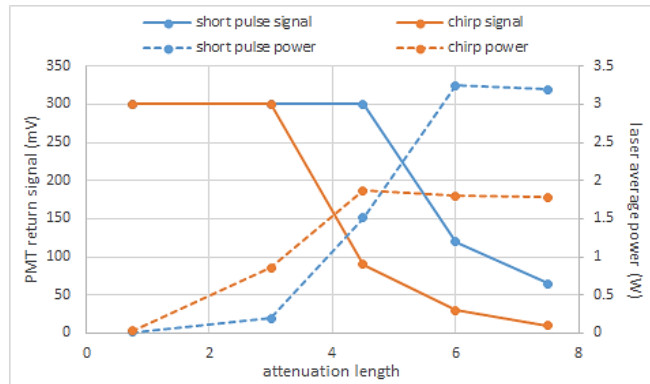

Fig. 2. Plots of the peak signal amplitude of the returns associated with the target measured by the PMT at the top surface of the wedding cake (solid lines, left axis), and the required average laser power needed to achieve those signal amplitudes (dashed lines, right axis) as a function of attenuation length. The blue curves are for the short pulse, and orange for the modulated pulse (chirp).

correlation peak’s location in time multiplied by c_0/n (where c_0 is the speed of light in vacuum and n is the refractive index of water) and dividing by two to account for the roundtrip.

Two peak detection algorithms were implemented to find the peak of the correlation function generated by the matched-filter operation. The baseline algorithm, denoted as “max peak” hereafter, found the sample with maximum value, and then performed a least squares analysis to fit a quadratic to a specified number of neighboring samples around the chosen sample. The location of the maximum value in the interpolated quadratic fit was then used to determine the range. Alternatively, another algorithm, denoted as “first peak” hereafter, did the same fitting procedure but chose the sample associated with the first peak after a user specified location in time around which to establish the collection of samples used for the quadratic fit. The user also specifies a threshold value for the peak defined in terms of a percentage of the magnitude of the absolute maximum peak. This peak detection method came into play when forward scattering caused returns from the target backboard to produce a larger peak in the matched-filter output than the one associated with the target feature of interest. Hereafter, the max peak algorithm is assumed to be used unless otherwise specified. Since the matched-filter output inherently provides well-defined and smooth peaks, the minimum number of samples (three) was used for the quadratic fit in both algorithms.

B. Short Pulse

For the short pulse scheme, since no gate was applied to the PMT to eliminate the backscatter response, a digital gate was used to ignore any portion of the return signal that occurred before a user specified point in time. Peak detection was then performed in the same manner as in the modulated pulse processing scheme. However, there were a number of ways to choose the signal on which the peak detection algorithm operated. The maximum range resolution was obtained by processing the digitized short pulse returns directly since they offered the narrowest width. While processing the returns directly offered the best range resolution, it also introduced “range noise” into the image. This was caused by a combination of shot noise and random pulse-to-pulse variations in the temporal shape of the pulse from pixel-to-pixel. Another approach was to apply a matched filter to the return signal (i.e. the same procedure performed with the modulated pulses), which can be thought of as a low-pass filter with a response ideally suited to the frequency content of the pulse. This increased the width of the peak, and therefore decreased the range resolution, but to a minimum extent, and also produced a smooth, well-defined peak with minimal range noise. In practice, by performing the matched-filter operation the correlation peak width was 1.55ns as opposed to the 1.3ns actual pulsewidth, resulting in a bandwidth of 645MHz compared to the 770MHz and 750MHz bandwidths of the short pulse returns and modulated pulse, respectively. The approach for the short pulse data was to perform the peak detection processing on both the directly digitized returns and the matched filtered returns to bracket the possible trade-off space between range resolution and range noise. It was found that it was only worth dealing with the additional range noise from processing the directly digitized returns in high turbidity cases when the slightly increased resolution allowed the first peak algorithm to recover some additional target feature information. Thus, data processed in this manner will only be presented in the highest turbidity scenario.

IV. RESULTS

In this section, images and temporal data generated using the modulated pulse approach will be denoted as "chirp" (referring to the 250-1000MHz linear frequency sweep of the RF encoded waveform), and the terms "modulated pulse" and "chirp" may be used interchangeably. Images and temporal data generated using the short pulse approach will be denoted "short". Additionally for the short pulse imagery, data processed using the matched-filter output will be denoted "xcorr" (referring to cross-correlation), and data processed using the returns directly will be denoted "return".

A. Image Analysis

In this section we will present the imagery obtained with both the short pulse and modulated pulse approaches over the tested range of turbidities. Images collected at each individual turbidity will be presented and discussed, followed by a summary over all turbidities to show the difference in the net effects of increased forward scatter between the two approaches.

Fig. 3 summarizes the results of the imagery in clean water (cz = 0.75, c = 0.1m^{-1}). 3D images using both the chirp and short pulses are given, as well as line profiles taken across a centrally located row of pixels in each image. The line profile labeled "clean reference" is taken from the chirp image in clean water and is therefore redundant in this case, but will be used for reference in forthcoming higher turbidity cases. These results show that both approaches performed identically well in clean water, and therefore a level playing field is established for the comparison.

Fig. 4 summarizes the results of the imagery taken at an attenuation length of 3.00 (c = 0.4m^{-1}). Some subtle rounding of the target features due to loss of range resolution from forward scattering is seen in both the short and chirp pulse images, however the short pulse image shows this artifact to a greater degree. This is more obvious when looking at the line profiles. Also, some reduction in range accuracy is noted by the biasing of the measured ranges to further distances across the entire target when compared to the clean reference line profile. This is most obvious when looking at the flat area of the target backboard between the cone and wedding cake. Again, this artifact affects the short pulse data to a greater extent than the chirp data. Quantifying the combination of these artifacts, the mean range error of the line profile data is 6.77mm and 2.59mm for the short pulse and chirp, respectively. The mean range error is calculated as the mean of the absolute value of the pixel-wise differences between the range data at the current turbidity and that of the clean water reference.

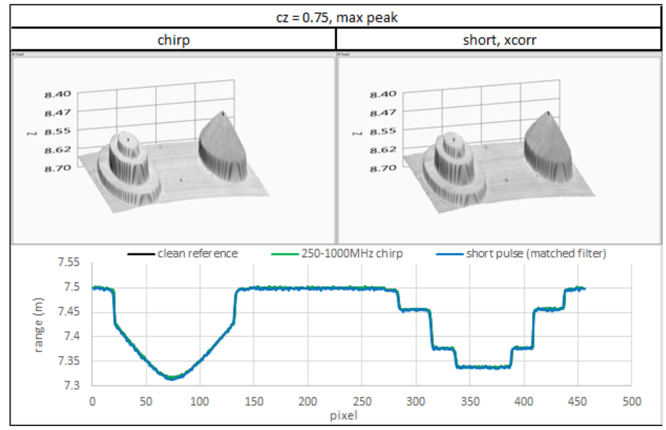

Fig. 3. Summary of results for 0.75 attenuation lengths showing the 3D images generated using the chirp (top left), short pulse (top right), and the line profiles of a centrally located row of pixels from those images plus the clean water reference image (bottom). This is the clean water case, therefore the "clean reference" and "250-1000MHz chirp" line profiles are identical. Results were generated using the MAX peak algorithm.

Fig. 5 summarizes the results of the imagery taken at an attenuation length of 4.50 (c = 0.6m^{-1}). Here there is a substantial amount of rounding of the target features in the

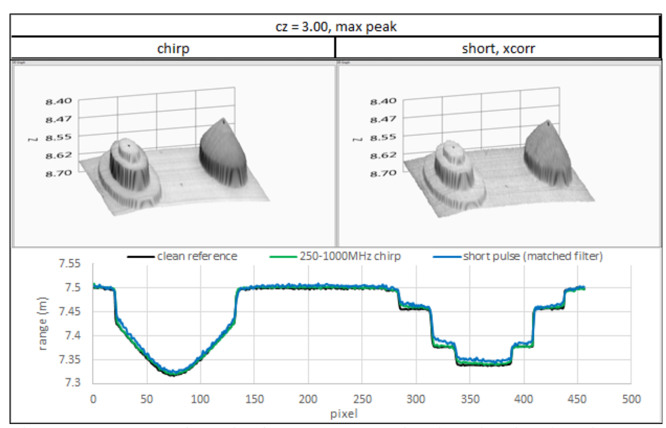

Fig. 4. Summary of results for 3.00 attenuation lengths showing the 3D images generated using the chirp (top left), short pulse (top right), and the line profiles of a centrally located row of pixels from those images plus the clean water reference image (bottom). Results were generated using the MAX peak algorithm.

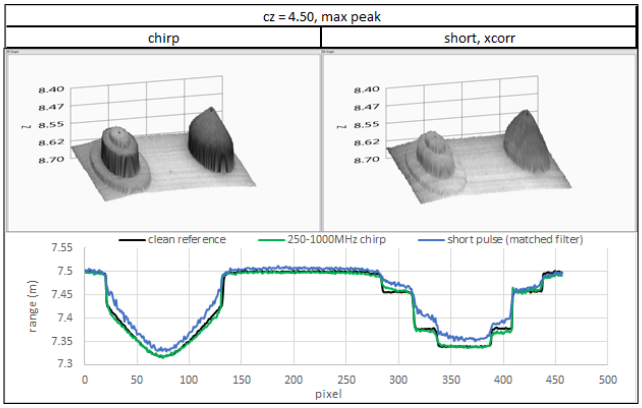

Fig. 5. Summary of results for 4.50 attenuation lengths showing the 3D images generated using the chirp (top left), short pulse (top right), and the line profiles of a centrally located row of pixels from those images plus the clean water reference image (bottom). Results were generated using the MAX peak algorithm.

short pulse image, whereas there is little difference in the sharpness of the target features in the chirp pulse images between attenuation lengths of 3.00 and 4.50. These observations are most obvious when comparing the chirp and short pulse line profiles to the clean reference in Fig. 4 and Fig. 5. There is also a further decrease in range accuracy in the short pulse image, evidenced by an increased separation between the chirp and short pulse line profiles in terms of bias toward further distances compared to the clean reference. The combination of the rounding and biasing artifacts leads to a "compressed" feel to the short pulse imagery. The mean range error of the line profiles is 13.41mm and 3.81mm for the short pulse and chirp, respectively.

Fig. 6 summarizes the results of the imagery taken at an attenuation length of 6.00 (c = 0.8m^{-1}). As a reminder, up to and including this point the max peak detection algorithm has been used exclusively. Here the returns from the target background were competing with those of the target features of interest. This is evidenced by varying degrees of absence of the target features between the images. The short pulse image processed using the matched-filter output shows an almost complete lack of target features since the max peak algorithm has chosen returns from the background almost exclusively. The short pulse image processed using the pulse returns directly shows what is essentially a noisier version of the same thing. The modulated pulse shows some degree of missed target features, but clearly is able to detect more target content than the short pulse approach. The spurious "spikes" seen in the modulated pulse image are a consequence of low SNR where the max peak algorithm encountered noise peaks that exceeded those of the target feature or the background. Another thing to notice is that the bias in the range measurements is now about the same between the short and chirp pulses. This leads one to conclude that the chirp is resistant to the range bias artifact up to some threshold turbidity (somewhere between attenuation lengths of 4.50 and 6.00), after which this resistance breaks down. The mean range error of the line profiles is 66.09mm, 70.62mm, and 62.92mm for the short pulse (xcorr), short pulse (return), and chirp, respectively.

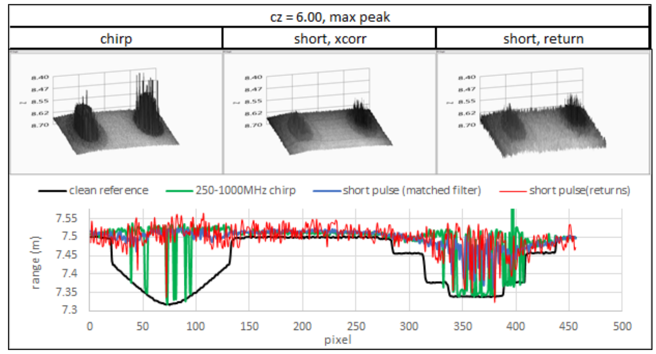

Fig. 6. Summary of results for 6.00 attenuation lengths showing the 3D images generated using the chirp (top left), short pulse processed using the matched-filter outputs (top middle), short pulse processed using the returns (top right), and the line profiles of a centrally located row of pixels from those images plus the clean water reference image (bottom). Results were generated using the MAX peak algorithm

Fig. 7 summarizes the results of the imagery taken at an attenuation length of 6.00, but now employing the first peak algorithm. In addition, Fig. 8 shows the temporal profiles of the received signals for the short pulse (xcorr and return) and chirp for a pixel at the top of the cone. In all cases, the first peak algorithm is successful in recovering target feature information to varying degrees. The least recovery is obtained for the short pulse image processed with the matched-filter output. This is because the pulse stretching induced by forward scatter leaves little separation between peaks associated with the background and the intended target features, as seen in Fig. 8. Since the matched-filter operation inherently widens the pulse slightly, processing the returns directly now offers an advantage in terms of range resolution and feature recovery, as seen in Fig. 8. However, this comes at the expense of significantly increased range noise, which is discussed in more detail in Section III-B. The modulated pulse image processed with first peak detection clearly is able to recover the most target information with no additional noise. This is due to the fact that the width of the correlation peak for the modulated pulse does not increase appreciably even in the presence of high forward scattering, allowing for continued separation of the background and target feature peaks, as seen in Fig. 8. However, even with first peak detection, the

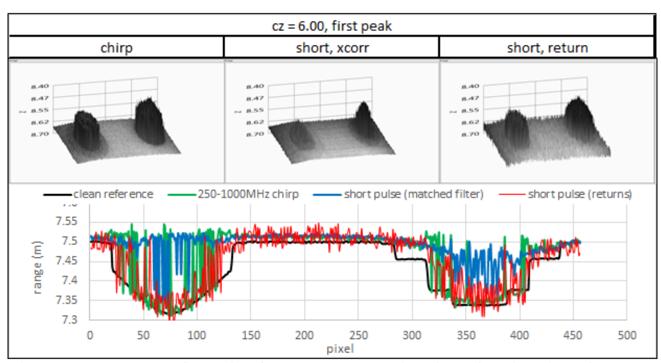

Fig. 7. Summary of results for 6.00 attenuation lengths showing the 3D images generated using the chirp (top left), short pulse processed using the matched-filter outputs (top middle), short pulse processed using the returns (top right), and the line profiles of a centrally located row of pixels from those images plus the clean water reference image (bottom). Results were generated using the FIRST peak algorithm.

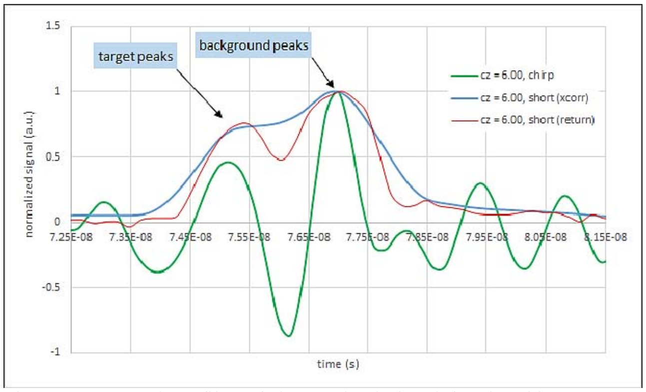

Fig. 8. Temporal profiles of the received signal for the chirp (green), short pulse xcorr (blue), and short pulse return (red) at cz = 6.00. Data is given for a pixel near the top of the cone.

modulated pulses are not immune to the range bias artifact at this turbidity level. Overall, the shapes of the target features in the modulated pulse image are still more representative of the actual shapes than those in the short pulse image, and comparatively free of noise. The mean range error of the line profiles is 61.75mm, 31.40mm, and 33.78mm for the short pulse (xcorr), short pulse (returns), and chirp, respectively. However, the mean range error may not be a good figure of merit for the short pulse (returns) data since averaging suppresses the range noise.

Fig. 9 summarizes the evolution of the line profiles over the tested range of turbidities for the chirped pulse (top) and short pulse (bottom). It is included to provide a better visualization of how the modulated pulse approach provides resistance to

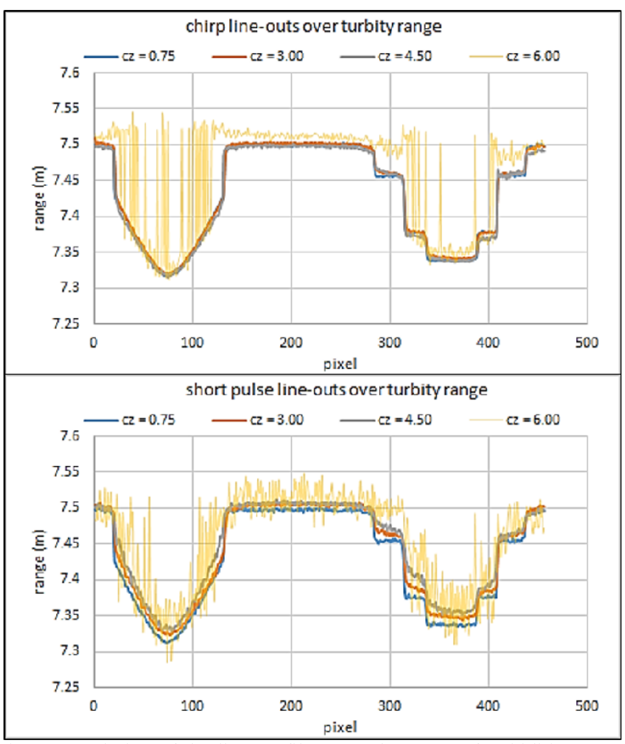

Fig. 9. Evolution of the line profiles over the range of turbidities tested for images generated using the chirp (top) and short pulse (bottom).

forward scatter effects, especially below attenuation lengths of 6.00. This is evident by noting the smaller relative change between the line profiles for the modulated pulse images (top) compared to those from the short pulse images (bottom) as turbidity increases.

B. *Temporal Analysis*

In this section, single pixel temporal data will be presented that substantiates the observations made in the imagery section. The three main observations are:

1) Forward scatter decreases range resolution

2) Forward scatter adds range bias (i.e. decreases range accuracy)

3) The modulated pulse approach is more resistant to these effects than the short pulse approach.

As shown in Fig. 10, temporal profiles corresponding to two different pixels in the image will be discussed. The first discussion will be based on a pixel in the center of the target backboard to highlight differences in the temporal profiles between the short pulse and the chirp when only one peak is present. The second discussion will be based on a pixel at the tip of the cone where competing peaks from the target feature and backboard are present.

1) Target Backboard

Fig. 11 shows measured temporal profiles (normalized matched-filter outputs) of the short pulse and chirp signals from a pixel at the center of the target backboard over the range of tested water turbidities (turbidity increasing working down the graph). Returns from the target backboard were chosen to be used here to eliminate any confusion of peaks associated with multiple target feature returns. One can clearly see that the short pulse correlation peaks stretch in pulsewidth in a continuous manner while the modulated pulse peaks maintain a fixed width as turbidity increases. This substantiates

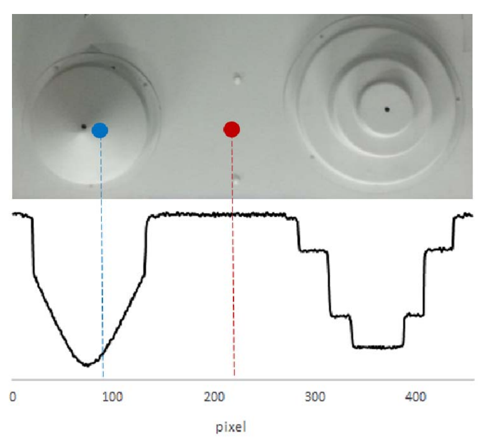

Fig. 10. Illustration of the two different pixel locations to be discussed for temporal analysis, one in the center of the target backboard (red) for analysis involving one return peak, and one on the tip of the cone (blue) for analysis involving multiple return peaks (target feature plus backboard).

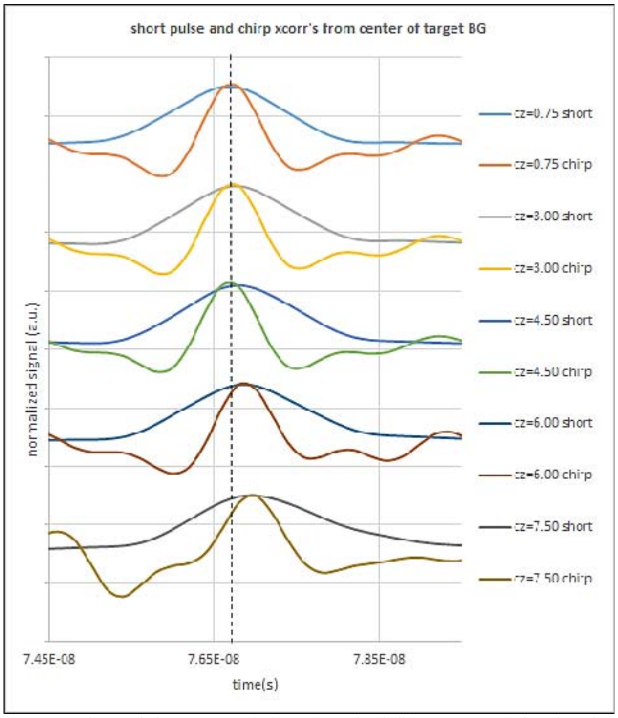

Fig. 11. Plots of the temporal data (matched-filter outputs) for the short pulse and chirp for a pixel located in the center of the target background. The plots at the top of the graph are in clean water, with turbidity increasing working down the graph. The data presented in Fig. 12 was measured using 8x interpolated versions of these temporal profiles.

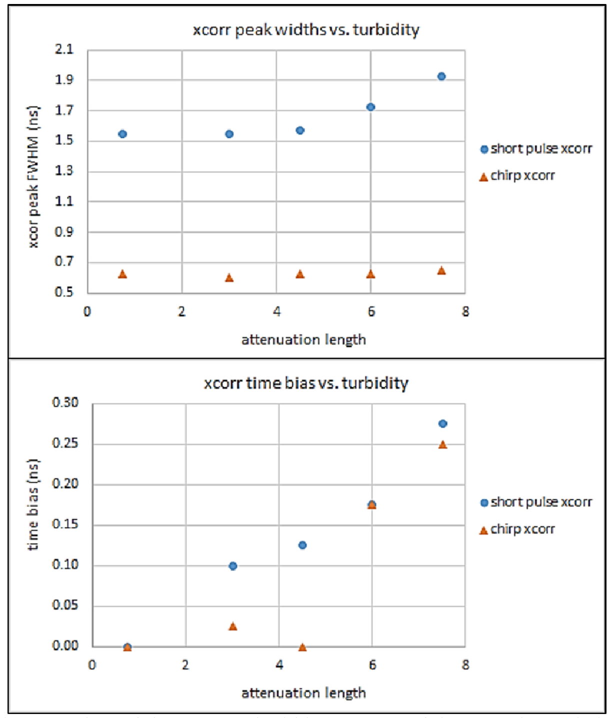

Fig. 12. Plots of the measured width (FWHM) of the central correlation peak as a function of turbidity for the chirp and short pulses (top), and location of the central correlation peak in time (bottom). Temporal data for a pixel in the center of the target background was used.

observations 1 and 3 from the image analysis. Additionally, one can see that the short pulse correlation peaks also continuously push out in time while the modulated pulse peaks only begin to exhibit this behavior above a threshold turbidity value. This substantiates observations 2 and 3. Fig. 12 quantifies the pulse stretching and range (time) bias artifacts. The top graph plots the measured FWHM of 8x interpolated versions of the matched-filter outputs given in Fig. 11 as a function of turbidity. The choice to work with the matched-filter outputs for the short pulse data (as opposed to the returns) was made because they have more well-defined shapes for determining the FWHM points. The graph clearly shows that the short pulse width is affected more as turbidity increases, leading to increased degradation in range resolution. The bottom graph plots the (interpolated) correlation peaks' locations in time as a function of turbidity. This helps to visualize resistance to the range bias artifact that the modulated pulse offers up to a certain threshold turbidity. The breakdown in this resistance is thought to be related to a phase delay induced within the chirp by the channel, but this still needs to be vetted with further measurements.

2) Target Feature

Fig. 13 is another summary of the evolution of the temporal profiles, but this time for a pixel near the top of the cone where the maximum range difference between a target feature and the backboard occurs. The graph shows overlaid plots of the short pulse matched-filter outputs, short pulse returns, and chirp matched-filter outputs as turbidity increases (moving down the graph). In addition to the behavior described above and shown in Fig. 11 and Fig. 12, the existence of multiple peaks is now seen in the short pulse data as the pixel registers returns from both the cone and the target background with increasing turbidity as a result of forward scattering. However, the modulated pulse data does not show any sign of the background return until the highest turbidity case is reached. This is a result of the forward scatter discrimination afforded by the high frequency content of the chirp and the coherent detection process. Comparing the profiles for the short pulse return and matched-filter output, it is clear that range resolution is improved when processing the returns directly, but again, this results in excess range noise. Even when taking this measure and accepting the additional range noise, the peak separation afforded by the modulated pulse is still better, leading to a higher degree of target feature recovery when using the first peak algorithm, as shown in Fig. 7. One disadvantage of the modulated pulse approach that is noticeable at the highest turbidity in Fig. 13 is that the sidelobes generated by the matched-filter could mistakenly be interpreted as target features under low SNR conditions. This may be able to be mitigated with wider bandwidth chirps, alternate RF coding schemes, and/or additional signal processing.

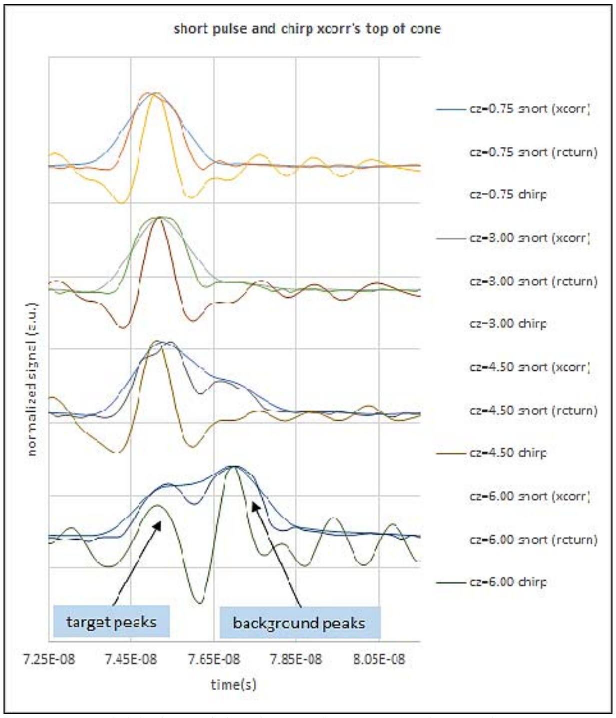

Fig. 13. Overlaid plots of the short pulse (xcorr), short pulse (return), and chirp temporal data for a pixel near the top of the cone (maximum range difference between target feature and the background). Turbidity increases working down the graph.

V. CONCLUSION

A detailed series of experiments has been completed that compares the capabilities of a line-scan 3D underwater optical imaging system armed with both short and modulated optical pulses. Comparisons were made in terms of each approach's resistance to the effects of forward scatter and were judged on overall image quality (i.e. feature representation), range resolution, and range accuracy as a function of water turbidity. The results show that the modulated pulse approach offers significant advantages in its resistance to forward scatter effects. These advantages are a result of the modulated pulse's fixed correlation peak width as a function of turbidity, and lack of time bias at moderate turbidities. In terms of processing, great attention has been paid to ensure that no disadvantage was placed on the short pulse data. In addition, the short pulse approach was allowed to maintain an SNR advantage by not limiting the return signal levels to those of the modulated pulse at higher turbidities. The purpose of this paper was not to challenge the effectiveness of current underwater 3D lidar imagers employing short pulse lasers, but rather to show proof that the modulated pulse approach can provide enhancements to the 3D image quality if incorporated into a given system. Finally, it should be noted that the results shown in this paper were for one particular modulated pulse scheme (the 250-1000MHz chirp). Since the modulated pulse system is extremely agile in terms of the frequency/phase content of the RF encoded waveforms, modulation schemes can easily be tailored to provide enhancements in different scenarios (e.g. channel frequency response, target feature sizes, etc.). Future work will focus on investigating the effect of different modulation schemes on system performance, and will incorporate targets of operational significance.

ACKNOWLEDGMENTS

The authors wish to acknowledge the Naval Innovative Science and Engineering (NISE) program (Section 219) which made this research possible.

REFERENCES

[1] F. R. Dalgleish, F. M. Caimi, W. B. Britton and C. F. Andren, "Improved LLS imaging performance in scattering-dominant waters," Proceedings of SPIE 7317 (2009).

[2] A. Weidemann, G. R. Fournier, L. Forand, P. Mathieu, "In harbor underwater threat detection/identification using active imaging," Proceedings of SPIE 5780, 59-70 (2005).

[3] S. O'Connor, L. Mullen and B. Cochenour, "Underwater modulated pulse laser imaging system", Optical Engineering 53(5), 051403 (May, 2014).

[4] B. Cochenour, L. Mullen, J. Muth, "Modulated pulse laser with pseudorandom coding capabilities for underwater ranging, detection, and imaging," Applied Optics, 50, 6168-6178 (2011).

[5] S. O'Connor, R. Lee, L. Mullen, B. Cochenour, "Waveform Design Considerations for Modulated Pulse Lidar", Proceedings of SPIE 9111 (2014).

[6] R. Lee, J. Nash, B. Cochenour, L. Mullen, "Pulse Compression Techniques to Improve Modulated Pulsed Laser Line Scan Systems", Proceedings of SPIE 9459 (May 19, 2015)

[7] Pellen, F., Intes, X., Olivard, P., Guern, Y., Cariou, J. and Lotrian, J., "Determination of sea-water cut-off frequency by backscattering transfer function measurement," J. Phys. D Appl. Phys. 33, 349-354 (2000).

[8] L. Mullen, A. Laux, and B. Cochenour, "Propagation of modulated light in water: implications for imaging and communications systems," Applied Optics, 48, 2607-2612 (2009).

[9] L. Mullen, D. Alley, and B. Cochenour, "Investigation of the effect of scattering agent and scattering albedo on modulated light propagation in water," Applied Optics, 50, 1396-1404 (2011).

[10] B. Cochenour, S. O'Connor, L. Mullen, "Suppression of forward-scattered light using high-frequency intensity modulation", Optical Engineering 53(5), 051406 (May, 2014).